

## Article

# Molecular Simulations of Unexplored Philippine Plant Constituents on the Inhibition of the Proinflammatory Marker NF-κB p50 Subunit

Jasmine U. Ting <sup>1,\*</sup>, Maria Carmen S. Tan <sup>1</sup>, Vincent Antonio S. Ng <sup>1</sup>, Stephani Joy Y. Macalino <sup>1</sup>, Virgilio C. Linis <sup>2</sup> and Glenn G. Oyong <sup>3,\*</sup>

<sup>1</sup> Department of Chemistry, De La Salle University, 2401 Taft Avenue, Malate, Manila 0922, Philippines; maria.carmen.tan@dlsu.edu.ph (M.C.S.T.); vincent.ng@dlsu.edu.ph (V.A.S.N.); stephani.macalino@dlsu.edu.ph (S.J.Y.M.)

<sup>2</sup> School of Multidisciplinary Studies, De La Salle-College of Saint Benilde, 2544 Taft Avenue, Malate, Manila 0922, Philippines; virgilio.linis@benilde.edu.ph

<sup>3</sup> Department of Physics, De La Salle University, 2401 Taft Avenue, Malate, Manila 0922, Philippines

\* Correspondence: jasmine.u.ting@outlook.com (J.U.T.); glenn.oyong@dlsu.edu.ph (G.G.O.)

**Abstract:** Inflammation serves as a pivotal defense mechanism orchestrated by the innate immune system to safeguard cellular health against adversities. Nonetheless, dysregulated inflammatory responses can precipitate chronic inflammatory ailments, notably autoimmune disorders. Central to this process are various pathways, with studies highlighting the pivotal role of transcription factors within the nuclear factor-kappa B (NF-κB) signaling pathway in disease onset and progression. This study concentrates on the p50 homodimer protein, a key transcription factor pivotal for the expression of proinflammatory cytokine genes. To explore potential inhibitors of p50, we conducted in silico procedures to investigate fifty-eight unexplored compounds, derived from plants indigenous to the Philippines. Initial screenings for compound feasibility, through drug-likeness analyses, yielded positive outcomes for 34 compounds. Subsequent docking analyses revealed six compounds exhibiting binding energies (ranging from  $-3.7$  to  $-4.2$  kcal/mol) akin to or lower than the positive control, dexamethasone ( $-3.7$  kcal/mol). These compounds include eudesm-11-en-4 $\alpha$ -O- $\beta$ -D-3-tigloyloxy-6-deoxy-glucopyranoside, wadeiol, grandiflorolide, eudesm-11-en-4 $\alpha$ -O- $\beta$ -D-3-senecioyloxy-6-deoxyglucopyranoside,  $\alpha$ -pinene-7 $\beta$ -O- $\beta$ -D-2-acetylglucopyranoside, and (2 $\alpha$ ,3 $\alpha$ ,5 $\alpha$ ,6 $\beta$ ,7 $\alpha$ ,8 $\alpha$ O)-6-[2-(3-furanyl)ethyl]-2a,3,4,5,5a,6,7,8,8a,8b-decahydro-2a,3-dihydroxy-6,7,8b-trimethyl-2H-naphtho[1-8-bc]furan-2-one. Interaction analyses revealed a common engagement of amino acid residues within the p50 DNA binding pocket, notably Arg57, Tyr60, Glu63, Lys244, Ala245, Pro246, Lys275, Arg308, Gln309, and Phe310, through hydrogen bonding, van der Waals forces, alkyl, and pi-alkyl interactions. Pharmacophore analysis underscored aromatic rings, hydroxyl, methyl, and methylene groups as pivotal for non-covalent interactions with p50. Additionally, root mean square fluctuation (RMSF) analysis demonstrated minimal residue fluctuations in p50 upon ligand binding compared to the ligand-free protein structure. In conclusion, the six shortlisted compounds exhibiting comparable binding affinities with dexamethasone hold promise as potential anti-inflammatory agents targeting the NF-κB p50 homodimer.

**Keywords:** inflammation; NF-κB; molecular docking; molecular dynamics; p50 inhibitor; Philippine plants; terpenoids



**Citation:** Ting, J.U.; Tan, M.C.S.; Ng, V.A.S.; Macalino, S.J.Y.; Linis, V.C.; Oyong, G.G. Molecular Simulations of Unexplored Philippine Plant Constituents on the Inhibition of the Proinflammatory Marker NF-κB p50 Subunit. *Crystals* **2024**, *14*, 438. <https://doi.org/10.3390/crust14050438>

Academic Editor: José Gavira

Received: 8 April 2024

Revised: 25 April 2024

Accepted: 30 April 2024

Published: 4 May 2024



**Copyright:** © 2024 by the authors. Licensee MDPI, Basel, Switzerland. This article is an open access article distributed under the terms and conditions of the Creative Commons Attribution (CC BY) license (<https://creativecommons.org/licenses/by/4.0/>).

## 1. Introduction

Plants deploy secondary metabolites as a defense mechanism against environmental stressors and invaders such as herbivores, bacteria, or viruses, with terpenoids serving as notable chemical defenses aiding in tissue repair [1]. These plant-derived compounds, including terpenoids and polyphenolic compounds, exhibit diverse bioactivities such as

anti-inflammatory and antioxidant properties, offering potential therapeutic benefits for combating various diseases in humans [2]. Terpenoids, for instance, act as natural inhibitors of NF- $\kappa$ B, effectively suppressing the NF- $\kappa$ B signaling pathway triggered by proinflammatory factors, thus serving as promising anti-inflammatory agents [3,4]. Additionally, polyphenolic compounds, among others, have been identified for their ability to alleviate inflammatory responses through multiple signaling pathways such as mitogen-activated protein kinase (MAPK), activator of transcription (STAT), and nuclear factor erythroid 2-related factor 2 (Nrf-2) [5].

Inflammation, a crucial defensive response orchestrated by the immune system, aims to eliminate pathogens, restore homeostasis, and facilitate tissue repair [6,7]. Immune cells release histamine, prostaglandins, and nitric oxide to enhance blood flow and recruit circulating leukocytes, while the release of proinflammatory cytokines (e.g., TNF- $\alpha$ , IL-1, and IL-6) promotes leukocyte migration into infected tissues by upregulating adhesion molecules on endothelial cells [8,9]. However, chronic inflammation can lead to cellular dysregulation, impaired proteolysis, tissue dysfunction, and apoptosis [3]. Addressing these symptoms necessitates medications to attenuate the exaggerated immune response, preventing adverse outcomes such as the overexpression of proinflammatory cytokines (cytokine storm) [4].

Over the past decade, numerous studies have underscored the pivotal role of the NF- $\kappa$ B signaling pathway in maintaining immune homeostasis [10]. Indeed, this pathway has emerged as a compelling therapeutic target for addressing chronic inflammation, autoimmune diseases, tumorigenesis, and even aspects of anti-aging [11–13]. NF- $\kappa$ B, a transcription factor, comprises five distinct members: p65 (RelA), RelB, RelC, p105/p50, and p100/p52. NF- $\kappa$ B signaling pathways are broadly categorized into two significant groups: canonical and non-canonical. Non-canonical activation of the NF- $\kappa$ B signaling pathway occurs through the tumor necrosis factor (TNF) receptor superfamily via a gradual yet sustained process. Central to non-canonical NF- $\kappa$ B pathways is the processing of p100, the precursor of p52, which is tightly regulated by two kinases, NF- $\kappa$ B-inducing kinase (NIK) and IkappaB kinase-alpha (IKK $\alpha$ ). This crucial step facilitates the release of the p52 homodimer from p100 and enables the formation of the RelB/p52 heterodimer, subsequently translocated into the nucleus to initiate the transcription of target genes involved in the inflammatory response.

In addition to regulating the inflammatory response, non-canonical pathways play a crucial role in the development of immune cells and lymphoid organs. Conversely, canonical activation of the NF- $\kappa$ B signaling pathway entails a relatively rapid and transient transcriptional activity primarily responsible for modulating proinflammatory genes [7,13]. A pivotal step in canonical activation involves the signal-induced phosphorylation of IkappaB (IkB) molecules by IKK. Subsequently, the p50/p65 heterodimer is liberated and permitted to translocate into the nucleus, where it binds to the promoter regions of target genes to initiate transcription [7]. Unlike other members of the NF- $\kappa$ B family, the transcriptional-inducing activity of the p50 homodimer is only activated upon heterodimer formation. In theory, molecules binding to the DNA binding region of either p65 or p50 have the potential to hinder binding to the target gene promoter region, thereby mitigating inflammation by impeding the transcriptional activation of proinflammatory cytokine genes. Furthermore, studies suggest that inhibiting p50 may not only alleviate chronic inflammation, but also exert effects on other diseases such as cancer [6].

To inhibit the activity of p50, Wang et al. (2009) devised a peptide that selectively binds to the DNA binding region of p50 [6]. Their proposed mechanism involves the downregulation of proinflammatory cytokines, as demonstrated in an in vitro trial using the human acute monocyte leukemia cell line (THP-1). Another study found that oligonucleotides binding to p50 hindered the protein's interaction with target genes at promoter regions, consequently enhancing the apoptosis of cancer cells [14]. These findings highlight p50 as a promising therapeutic target for alleviating the overexpression of proinflammatory cytokines, thereby regulating inflammatory responses and mitigating carcinogenesis in

conditions of chronic inflammation, including autoimmune diseases, diabetes, and hypertension. Furthermore, anti-inflammatory compounds play a crucial role in managing acute infections caused by bacterial and viral pathogens, particularly in suppressing the potentially fatal “cytokine storm”. Incorporating terpenoids into the p50 DNA binding site inhibits the NF- $\kappa$ B transcription factor from binding to the promoter region of target genes, ultimately preventing the transcriptional activation of proinflammatory cytokine genes (Figure 1) [6,7,10–12].

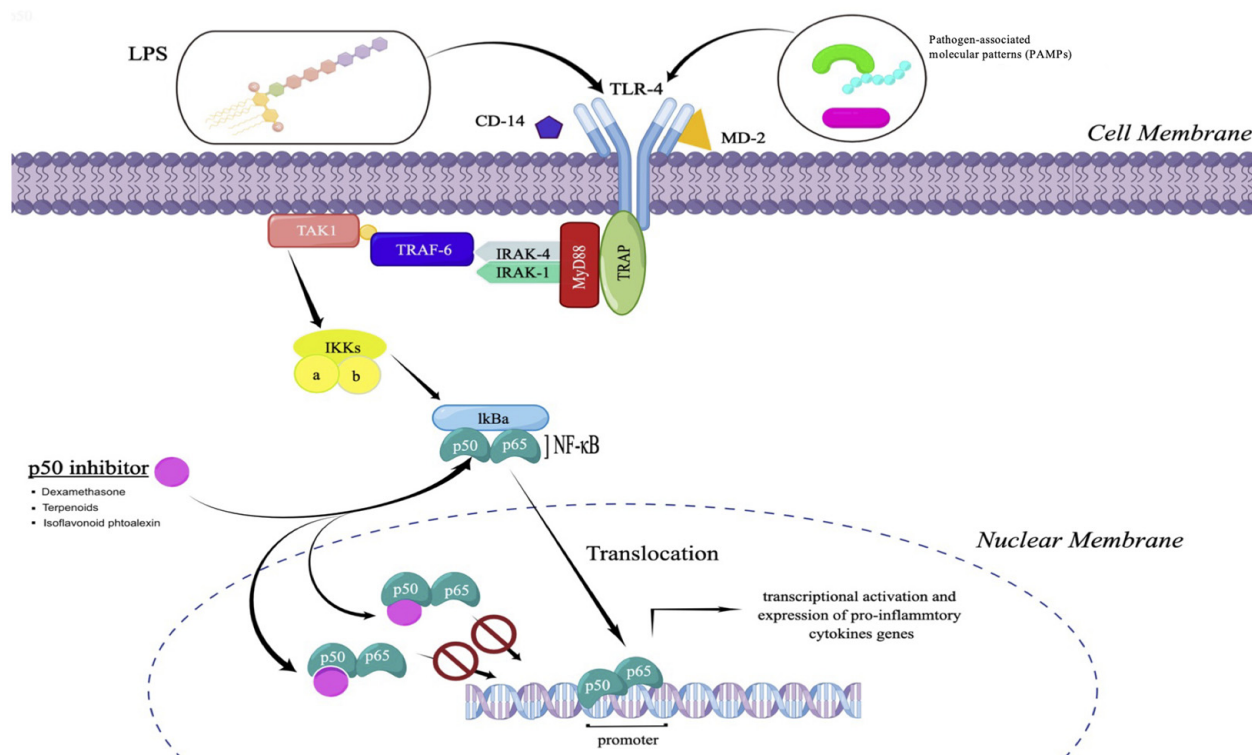


**Figure 1.** Proposed mechanistic pathway of terpenoids inhibiting the canonical NF- $\kappa$ B pathway by blocking the DNA binding region of the p50 homodimer (drawn in FigDraw).

The primary objective of this study was to utilize in silico computer-aided drug design (CADD) techniques to screen for potential anti-inflammatory agents. This involved assessing druggability, determining binding affinities with the p50 homodimer, and evaluating binding stability through molecular dynamics simulation. Given the well-documented anti-inflammatory properties of terpenoids, our aim was to establish preliminary evidence regarding their potential anti-inflammatory activity at the in silico level, thus laying the groundwork for future in vitro and in vivo experiments. This strategic approach in drug discovery offers a cost-effective means of efficiently shortlisting compounds for further analysis, bypassing the need for blind testing of the entire compound library. Importantly, to the best of our knowledge, there are currently no published reports detailing the potential bioactivities of these compounds based on a comprehensive literature search.

## 2. Materials and Methods

### 2.1. Terpenoids

Fifty-eight terpenoids selected for this study were previously reported as either new (derivatives of known skeletal structures) or novel (constituents with newly discovered unique skeletal structures) compounds isolated from twenty-seven species and one hybrid of plants collected in the Philippines by Ragasa et al. (1993–2020) [15–45]. Table S1 presents a comprehensive list of these compounds along with the plant species and hybrid from which they were isolated.

## 2.2. Preparation of the p50 3D Structure

The pdb file of the human p50 homodimer (PDB ID:1SVC) was obtained from the Protein Data Bank (PDB) database (<https://www.rcsb.org/>, accessed on 11 July 2022). Prior to docking analysis, water molecules, native ligands (DNA) in the binding site, and other heteroatoms were removed from the protein using BIOVIA Discovery Studio Visualizer v.21.2 (Dassault Systèmes, Waltham, CA, USA). The binding site was defined with XYZ center coordinates (27.702003, 30.851276, 27.702665) and size dimensions of  $20 \times 20 \times 20 \text{ \AA}$ , respectively. Polar hydrogens and Kollman charges were added using AutoDockTools (ADT) v.1.5.6 (Scripps Research, CA, USA), and the prepared protein was saved in pdbqt format. The stability and reliability of the optimized p50 3D protein were further validated using Zlab (UMass Chan Medical School, Worcester, MA, USA, <https://zlab.umassmed.edu/bu/rama/>, accessed on 11 July 2022) and Verify 3D and ERRAT (UCLA-DOE, Los Angeles, CA, USA, <https://saves.mbi.ucla.edu/>, accessed on 11 July 2022) servers.

## 2.3. Preparation of Ligands and Pharmacokinetics Investigation

The dexamethasone (CID:5743) control and 4 out of 58 compounds with available structures in the PubChem database (<https://pubchem.ncbi.nlm.nih.gov/>, accessed on 11 July 2022) were downloaded as 3D sdf files. The structures of the remaining 54 compounds were drawn using ChemSketch (2020) Version 12.01 (ACD/Labs, Toronto, ON, Canada) and optimized in the 3D Optimization feature [46]. The optimized structures were saved in mol format and converted to pdbqt format via OpenBabel v.2.4.0 (GPL v2, SourceForge, San Diego, CA, USA, <https://sourceforge.net/projects/openbabel/>, accessed on 11 July 2022) [47]. Additionally, the SMILES connotations of all compounds were obtained using OpenBabel and uploaded to ADMETlab 2.0 (<https://admetmesh.scbdd.com/contact/>, accessed on 12 July 2022) to predict their drug-likeness and pharmacokinetic properties [48]. Only compounds that passed Lipinski's rule of five underwent further analysis to determine their anti-inflammatory potential via in silico p50 docking.

## 2.4. Molecular Docking Analysis

AutoDock Vina 1.1.2 (Scripps Research, CA, USA) was employed for docking the ligands into the defined DNA binding site of p50, with grid dimensions set at  $20 \times 20 \times 20 \text{ \AA}$  along the x, y, and z axes centered at coordinates (27.702003, 30.851276, 27.702665), and default exhaustiveness was set at 8 [49]. The resulting binding energies (kcal/mol) were recorded and tabulated. Compounds with comparable or lower binding energy (indicating higher affinity) than dexamethasone (best-docked) were selected for further analysis in Discovery Studio Visualizer and molecular dynamics simulation. The amino acid residues interacting with the ligand were automatically generated in Discovery Studio Visualizer by defining the protein and ligand parameters as default.

## 2.5. Molecular Dynamics Simulation

The dynamic movements of the p50 apo protein, as well as p50–dexamethane and p50–12 (top docked ligand) complexes, were investigated. Protein and ligand topologies were generated using CHARMM-GUI (<https://charmm-gui.org/>, accessed on 15 March 2025), where the complexes were enclosed in a water box with an edge distance of 10 Å. KCl ions were added to neutralize any present charges, and the CHARMM36 all-atom force field was applied to all systems. Using Groningen Machine for Chemical Simulation (GROMACS) 2022 [50,51], all systems underwent minimization using the steepest descent algorithm at 5000 steps. A two-step equilibration process was applied to equilibrate the system at approximately 310.15 K (NVT) and 1 bar (NPT), using the Nose–Hoover temperature coupling method and Parrinello–Rahman pressure coupling, respectively. The resulting systems were subjected to 200 ns production runs with a timestep of 2 fs. Protein energy network (PEN) analysis was performed using gRINN to determine any changes in intramolecular communication of the protein structure due to ligand binding. Trajectories

were visualized using PyMOL, and relevant graphs were plotted in XMGrace. Hydrogen bond analysis was performed using Visual Molecular Dynamics (VMD) [52]. Molecular dynamics experiments were performed using a GPU with AMD Ryzen 7 3800X 8-core processor, 64 GB RAM, and PNY GeForce RTX 2060 SUPER 8 GB [53].

### 2.6. Pharmacophore Modeling

The mol2 files of the best-docked compounds with high potential were generated by OpenBabel and submitted to the PharmaGist server (<https://bioinfo3d.cs.tau.ac.il/PharmaGist/>, accessed on 22 July 2022) to generate the pharmacophore descriptor of each compound [54]. These descriptors represent the structural features critical for effective interaction or binding with the biological protein target. Subsequently, the pharmacophore descriptors were visualized in BIOVIA Discovery Studio Visualizer [55].

## 3. Results

### 3.1. Structural Validation of the Processed p50 Protein

To ascertain the reliability of the generated three-dimensional (3D) model, the processed p50 protein underwent validation through various algorithms. The Ramachandran plot revealed that 94.36% of the amino acids resided within the favorable region, indicating reasonable main chain and side chain conformations of the processed p50 protein (Figure 2A). Additionally, further evidence of the 3D model's reliability was substantiated by results obtained from Verify3D (Figure 2B) and ERRAT (Figure 2C) analyses. Verify3D analysis revealed that 99.04% of the residues exhibited a 3D/1D ratio greater than 0.2, suggesting high compatibility between the 3D structure and its 1D sequence. The scores on the plot rarely exceeded 0.1, indicating well-folded protein structure [56,57]. Moreover, the overall quality factor of the model, as determined by ERRAT, exceeded 50% (80.537%), affirming the acceptability of the structure and non-bonding atom–atom interactions within the model.

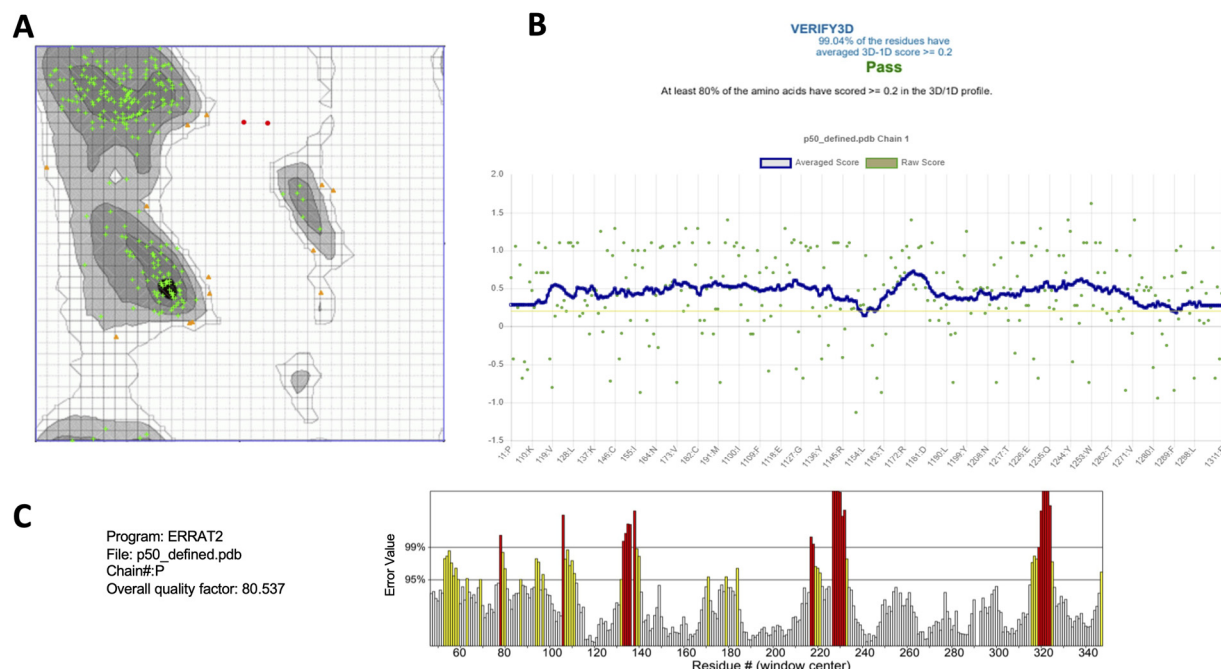


**Figure 2.** Structural validation of the processed p50 protein: (A) Ramachandran plot: black dark grey/light grey represents region for highly preferred conformation ( $\Delta \geq -2$ ); white with black grid represents the region for preferred conformation ( $\Delta \geq 4$ ); white with grey grid represents the region for questionable conformations ( $\Delta \leq -4$ ); highly preferred observation shown as green crosses: 251 (94.361%); preferred conformation shown in brown triangles: 13 (4.887%) and unpreferred conformation shown as red circles: 2 (0.752%); (B) Verify3D; and (C) ERRAT.

### 3.2. In Silico Investigation of the Anti-Inflammatory Potential of Compounds

In our study, we screened 58 unexplored compounds, isolated by Ragasa et al. from 1993 to 2020, sourced from locally available plants, as potential candidates for in silico analyses (Table S1). Initial qualification criteria involved applying Lipinski's rule of five (LO5) to select candidates with high oral absorption properties [58]. Following screening, 34 candidates (Table S1) met the criteria for druggability. Subsequently, docking analysis revealed that only six compounds exhibited binding energies equal to or less than the positive controls dexamethasone ( $-3.7 \text{ kcal/mol}$ ), chlorogenic acid ( $-3.5 \text{ kcal/mol}$ ), and humulene ( $-3.1 \text{ kcal/mol}$ ). Despite dexamethasone's known role as an inhibitor of p65 and the glucocorticoid receptor, it was included as a positive control due to its well-documented anti-inflammatory activity [59,60]. Notably, no studies support the availability of anti-inflammatory drugs in the market known to suppress p50, necessitating the consideration of several compounds in this study as positive controls to ensure the reliability of predicted p50 inhibitory activity among the candidates [61]. One such control was chlorogenic acid, which reportedly decreases the availability of p50 subunits for its anti-inflammatory activity [62]. Another positive control, humulene (C3), a sesquiterpene, was chosen for its potent anti-inflammatory activity across various inflammatory pathways [63]. The flow of activities leading to the selection of the final six candidate compounds, along with their corresponding binding energies, is presented in Figure 3 and Table 1.

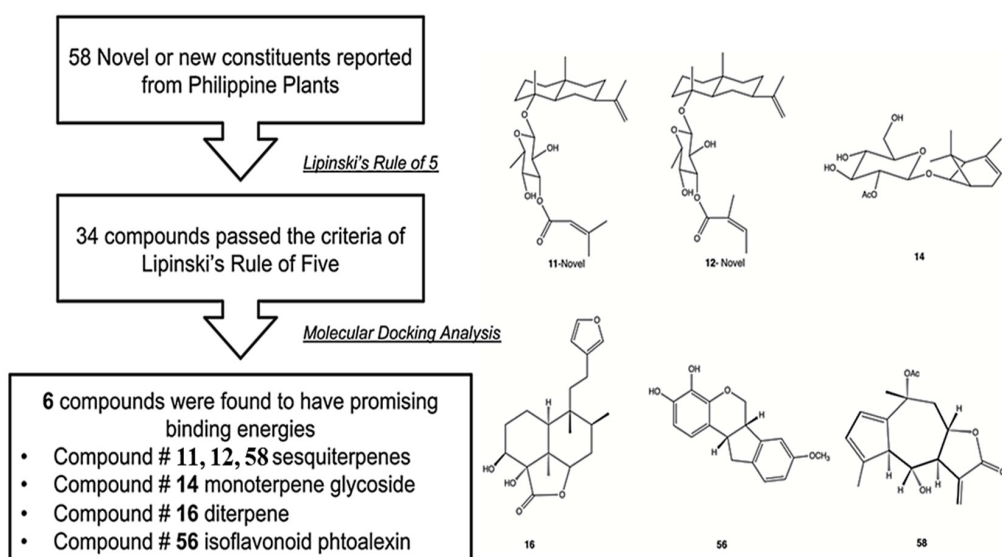


**Figure 3.** Workflow of the in silico procedure in selecting potential a p50 inhibitor from unexplored plant-derived compounds.

The p50 protein, comprising 310 amino acid residues, consists of two distinct domains, the N-terminal (43–244) and C-terminal (250–354) domains, linked by an interdomain linker (245–249). Previous studies have shown that both domains interact with the main groove of DNA through hydrogen bonding with the sugar phosphates or ribose [57]. In our study, ten amino acid residues of p50 were found to interact with the compounds (Figure 4; Supplementary Figures S1–S5): Arg57, Tyr60, Glu63, Lys244, Ala245, Pro246, Lys275, Arg308, Gln309, and Phe310. Nine of these residues (Arg 57, Tyr60, Glu63, Lys244, Ala245, Pro246, Lys 275, Arg308, and Gln309) have been reported to play essential roles in the binding of the protein with DNA [64]. As compared to the positive control (dexamethasone), the compounds exhibiting binding energies ranging from  $-3.7$  to  $-4.2 \text{ kcal/mol}$  may act as candidate competitive inhibitors, potentially preventing p50 from binding with DNA. By interacting with the responsible amino acid in DNA binding, the compounds that yield the lowest binding energy do have the higher the binding affinity to the protein [65].

**Table 1.** The binding energies of the six shortlisted compounds and their drug-likeness.

Compound Name	Code	Binding Energy (kcal/mol)	Molecular Formula	Lipinski's Rule of Five *				TPSA (Å) ≤140
				MW (Da)	Log P ≤5	HBA ≤10	HBD ≤5	
Dexamethasone ** (CID:5743)	C1	−3.7	C <sub>22</sub> H <sub>29</sub> O <sub>5</sub> F	394.51	1.9	5	3	94.8
Chlorogenic acid (CID:1794427)	C2	−3.5	C <sub>16</sub> H <sub>18</sub> O <sub>9</sub>	354.10	0.3	9	6	164.75
Humulene *** (CID: 5281520)	C3	−3.1	C <sub>15</sub> H <sub>24</sub>	204.19	5.2	0	0	0
eudesm-11-en-4 <sup>α</sup> -O-β-D-3-senecioyloxy-6-deoxyglucopyranoside	11	−3.9	C <sub>26</sub> H <sub>42</sub> O <sub>6</sub>	464.64	4.7	6	2	85.2
eudesm-11-en-4 <sup>α</sup> -O-β-D-3-tigloyloxy-6-deoxy-glucopyranoside	12	−4.2	C <sub>26</sub> H <sub>42</sub> O <sub>6</sub>	464.64	4.7	6	2	85.2
α-pinene-7β-O-β-D-2-acetylglucopyranoside	14	−3.9	C <sub>18</sub> H <sub>28</sub> O <sub>5</sub>	314.37	0.2	6	4	99.4
(2a <sup>β</sup> ,3 <sup>α</sup> ,5a <sup>β</sup> ,6 <sup>β</sup> ,7 <sup>α</sup> ,8a <sup>α</sup> )-6-[2-(3-furanyl)ethyl]-2a,3,4,5,5a,6,7,8,8a,8b-decahydro-2a,3-dihydroxy-6,7,8b-trimethyl-2H-naphtho[1-8-bc]furan-2-one	16	−3.7	C <sub>20</sub> H <sub>28</sub> O <sub>5</sub>	348.44	2.7	5	2	79.9
Wadeiol	56	−4.0	C <sub>16</sub> H <sub>13</sub> O	286.28	2.7	5	2	68.2
Grandiflorolide	58	−4.0	C <sub>17</sub> H <sub>20</sub> O <sub>5</sub>	304.34	1.7	5	1	72.3

\* MW: molecular weight; Log P: lipophilicity; HBD: hydrogen bond donor; HBA: hydrogen bond acceptor; TPSA: topographical surface area; \*\* marketed drug control; \*\*\* terpenoid control.

Compound **12** demonstrated the strongest affinity (lowest binding energy) to p50, while compound **16** exhibited the weakest. The two-dimensional (2D) and 3D representations of binding interactions, ligand–protein interacting residues, hydrophobicity, and H-bond surfaces, as well as Ramachandran plots, are depicted in Figure 4 and Supplementary Figures S1–S5. The p50 interacting residues based on 2D and 3D displays exhibit five amino acids (Glu63, Lys244, Ala245, Pro246, and Phe310) which are found in the  $\alpha$ -helix region of the protein based on the Ramachandran plot. Three (Arg 57, Tyr 60, and Lys 275) and two (Arg 308 and Gln 309) are located in the  $\alpha$ -sheet and left-handed helix, respectively. Among the 10 amino acids, Lys244 and Lys275 interacted with the compounds through conventional hydrogen bonding, except for sesquiterpene glycosides (**11** and **12**), which was via alkyl interaction (Supplementary Figure S1 and Figure 4), and clerodane diterpene (**16**), which was by pi–cation interaction (Supplementary Figure S3). In contrast, Tyr 60 displayed alkyl interactions with compounds **11**, **12**, and **14**, and a pi–pi T-shaped interaction with compound **56**. Both Tyr 60 and Pro 246 were found to engage in alkyl interactions with compound **11**, while Arg308 interacted with compound **12**. Moreover, Arg308 and Pro246 formed interactions with other compounds, involving conventional hydrogen bonding (Arg308 with **11** and **58**) and carbon–hydrogen bonding (Pro246 with **14**). Notably, only Phe310 was observed to interact with compound **12** through a pi–alkyl interaction. Due to their polarity, hydrophilic amino acids (Lys 244 and Lys 275) were primarily involved in interactions with hydrogen-donating or -accepting sites of the ligands. Consequently, Table 2 summarizes the protein residues engaged in ligand binding along with the types of non-covalent interactions. These 10 amino acid residues exhibit distinct interactions with the ligands, as determined by the pharmacophore properties of each compound. The

specific pharmacophore descriptors for each compound are illustrated in Figure 5 and listed in Table 3.

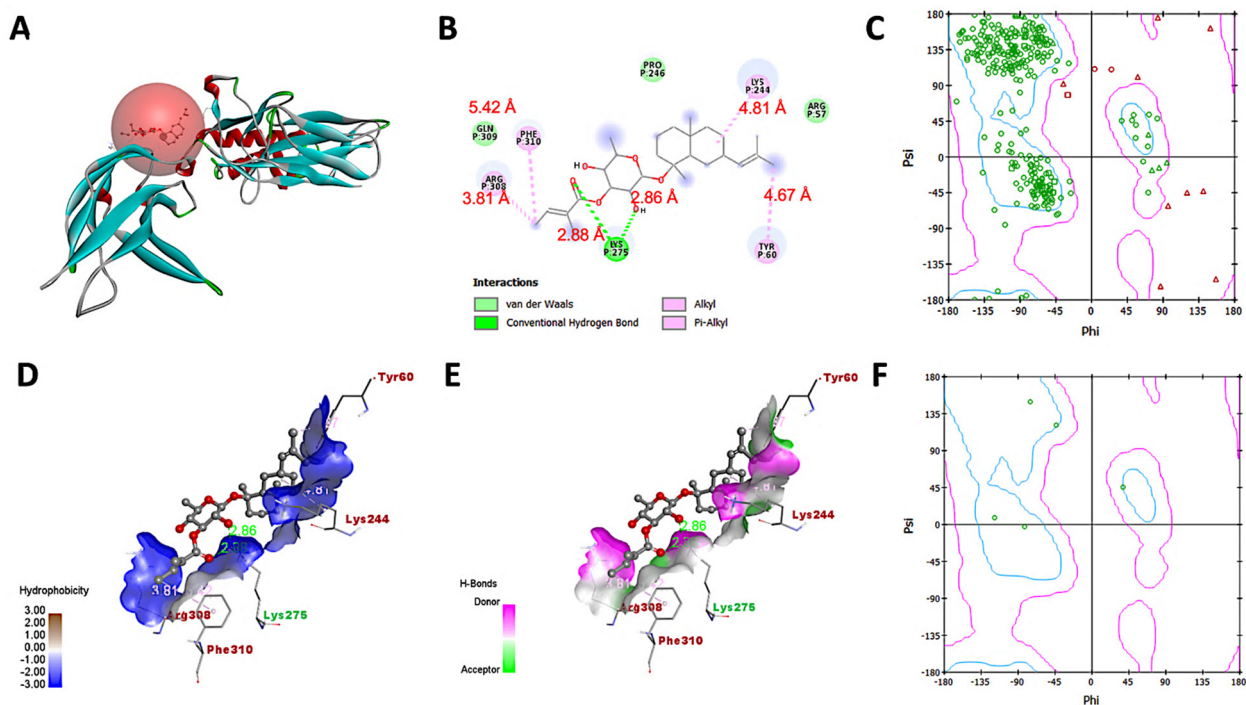


**Figure 4.** Binding interaction of p50 and compound 12: (A) ligand binding sphere and the p50 protein; (B) two-dimensional display of the interaction; (C) Ramachandran plot of p50; (D) hydrophobic property of the binding pocket; (E) H-bond property of the binding pocket; and (F) Ramachandran plot of ligand-interacting amino acid residues.

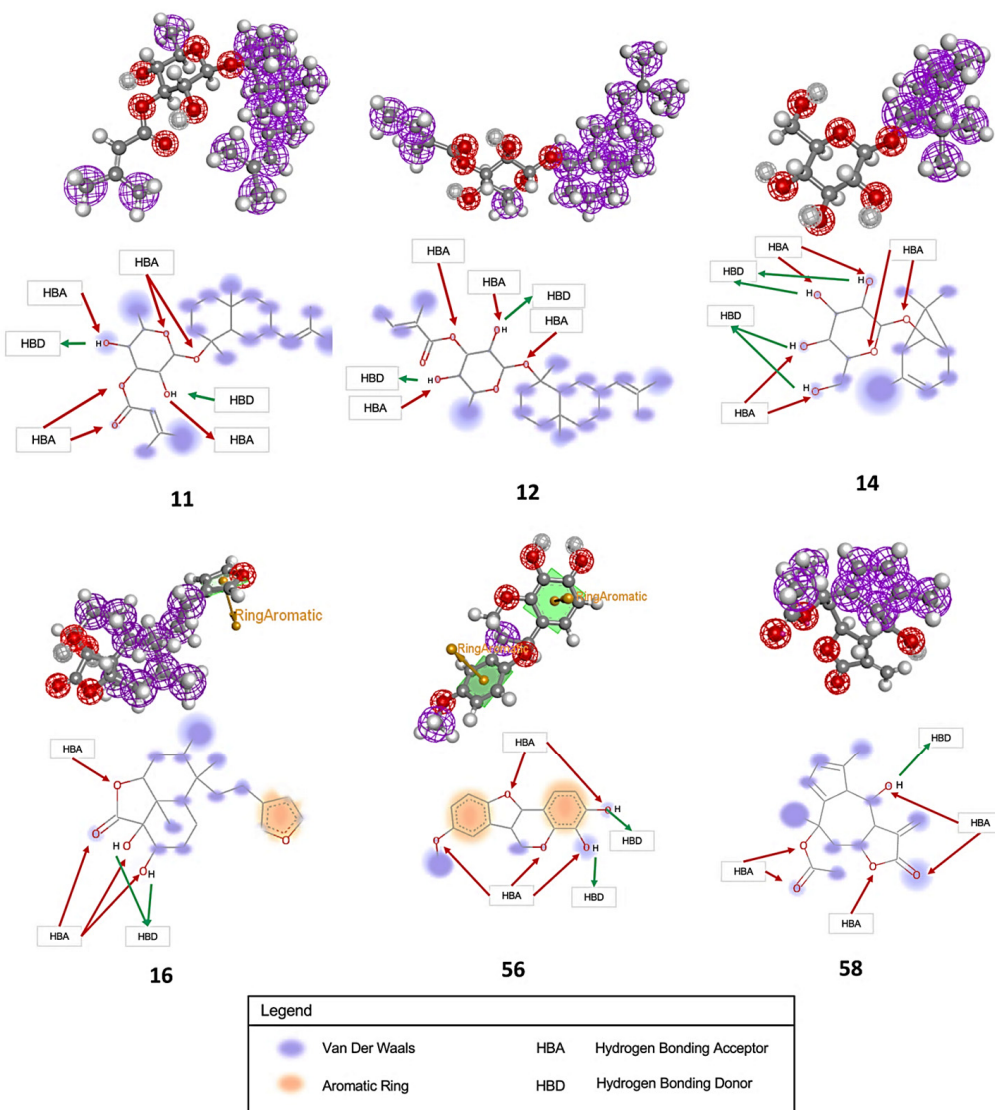
**Table 2.** Amino acid residues of the p50 homodimer interacting with the top six (6) binding phytochemicals obtained from different plants.

Compound	Interacting Residues	Protein Residues Involved in					
		Hydrogen Bonding	Van der Waals	Alkyl and/or π-alkyl	Carbon Hydrogen Bonding	π-Cation	π-π T-Shaped
11	Arg 57, Tyr 60, Glu 63, Lys 244, Ala 245, Pro 246, Lys 275, Arg 308	Lys 275 (1.85 Å), Arg 308 (2.39 Å)	Arg 57, Glu 63, Ala 245	Tyr 60 (5.03 Å), Lys 244 (4.69 Å), Pro 246 (5.38 Å)	n.a.	n.a.	n.a.
12	Arg 57, Tyr 60, Lys 244, Pro 246, Lys 275, Arg 308, Gln 309, Phe 310	Lys 275 (2.86 Å)	Arg 57, Pro 246, Gln 309	Tyr 60 (4.67 Å), Lys 244 (4.81 Å), Arg 308 (3.80 Å), Phe 310 (5.41 Å)	n.a.	n.a.	n.a.
14	Arg 57, Tyr 60, Glu 63, Lys 244, Ala 245, Pro 246, Lys 275	Lys 244 (2.42 Å), Lys 275 (2.16 Å)	Arg 57, Glu 63, Ala 245	Tyr 60 (5.47 Å)	Pro 246 (3.50 Å)	n.a.	n.a.
16	Lys 244, Lys 275, Arg 308, Phe 310	Lys 244 (2.33 Å)	Arg 308, Phe 310	n.a.	n.a.	Lys 275 (4.24 Å)	n.a.

**Table 2.** Cont.

Compound	Interacting Residues	Protein Residues Involved in					
		Hydrogen Bonding	Van der Waals	Alkyl and/or $\pi$ -alkyl	Carbon Hydrogen Bonding	$\pi$ -Cation	$\pi$ - $\pi$ T-Shaped
56	Arg 57, Tyr 60, Glu 63, Lys 244, Pro 246, Lys 275	Lys 244 (2.03 Å)	Arg 57, Glu 63, Lys 275	Pro 246 (4.20 Å)	n.a.	n.a.	Tyr 60 (4.80 Å)
58	Lys 275, Arg 308, Gln 309, Phe 310	Lys 275 (2.18 Å), Arg 308 (2.16 Å)	Gln 309, Phe 310	n.a.	n.a.	n.a.	n.a.

n.a.: Not applicable.

**Figure 5.** Pharmacophore descriptors of the ligands' predicted druggability and the nature of their interactions with the binding amino acid residues of the target protein.

**Table 3.** Details of pharmacophore descriptors of the six compounds generated by PharmaGist.

Compound	Features	Pharmacophore Descriptors			
		Aromatic	Hydrophobic	Hydrogen Donors	Hydrogen Acceptors
11	31	0	23	2	6
12	30	0	22	2	6
14	22	0	12	4	6
16	21	1	13	2	5
56	11	2	2	2	5
58	15	0	9	1	5

The generated pharmacophore features confirmed the presence of structural descriptors that direct the type of interactions involved with the binding amino acid residues. These descriptors also predict the druggability of the compounds based on Lipinski's criteria and are therefore important in drug development, particularly in the improvement of the drug by structural modifications. In Figure 6, the overlapped best-docked pose of the six short-listed compounds with dexamethasone occupying the same binding region are presented.

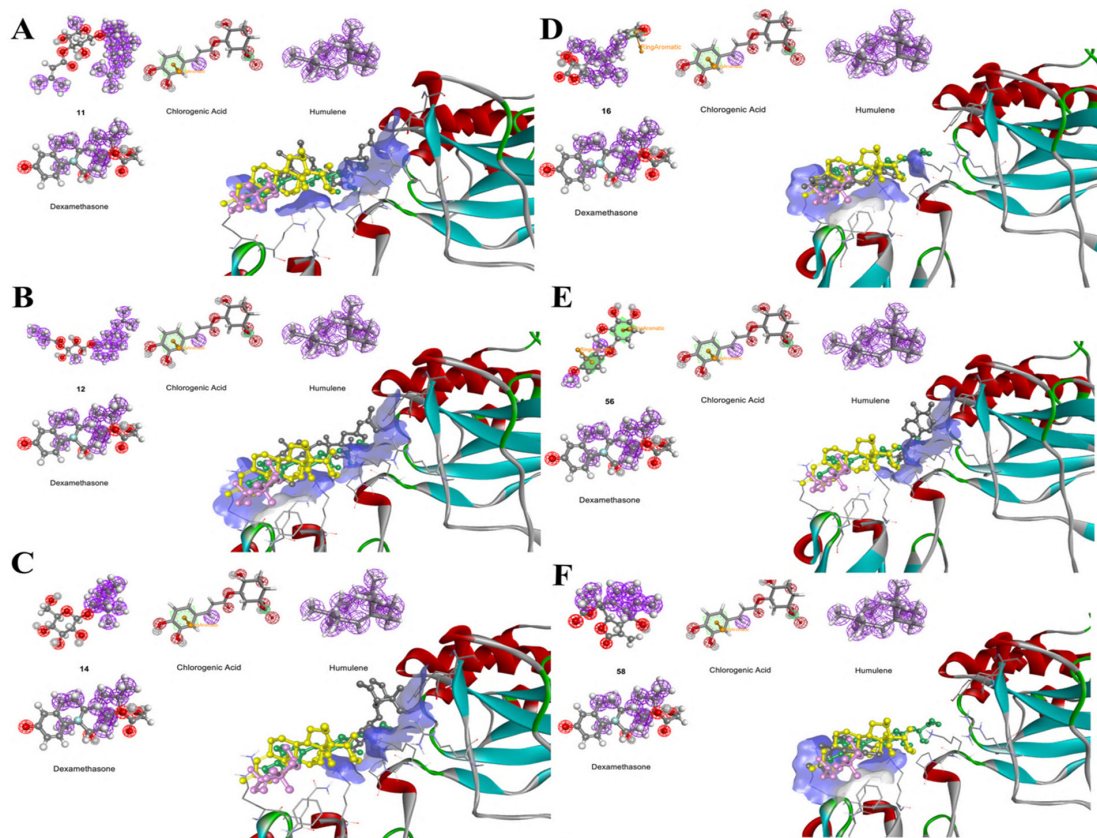


**Figure 6.** Comparison of pharmacophore descriptors between ligands and dexamethasone and the resulting overlapping displays of the best-docked poses of the ligands (gray) with dexamethasone (yellow), humulene (pink), and chlorogenic acid (green); (A–F), compounds 11, 12, 14, 16, 56, and 58.

### 3.3. Molecular Dynamics Simulation

As a response to ligand binding, a protein's flexibility can be altered, potentially affecting conformational entropy and the distribution of protein dynamics [66–68]. To explore the repercussions of ligand binding on the p50 protein, molecular dynamics simulations (MDSs) were conducted for the apoprotein (unbound protein), p50–dexamethasone (control), and p50–12 (top docked ligand).

The root mean square deviation (RMSD) showed large conformational changes for both the dexamethasone- and compound-**12**-bound structures as compared to the apo structure. Additionally, root mean square fluctuation (RMSF) analysis across all systems revealed notable alterations in protein flexibility upon ligand binding (Figure 7). Specifically, regions where the  $\Delta\text{RMSF}$  ( $| \text{bound} - \text{unbound} |$ ) exceeded 0.5 indicated significant changes induced by ligand binding [69]. The comparison between dexamethasone and compound **12** bindings showcased distinct patterns of residue fluctuation in the p50 protein. These differences likely stem from structural disparities between the compounds, influencing the protein's conformational landscape differently. However, both ligands induced increased flexibility in residues 151–163 and 188–195, while enhancing rigidity in residues 91–98, 128–131, 228–230, and across the C-terminal half. This suggests that ligand binding may restrict movement within the C-terminal lobe of p50. Combined, these findings imply that both compounds can potentially inhibit p50 activity by destabilizing its overall conformation by targeting similar areas within the protein.

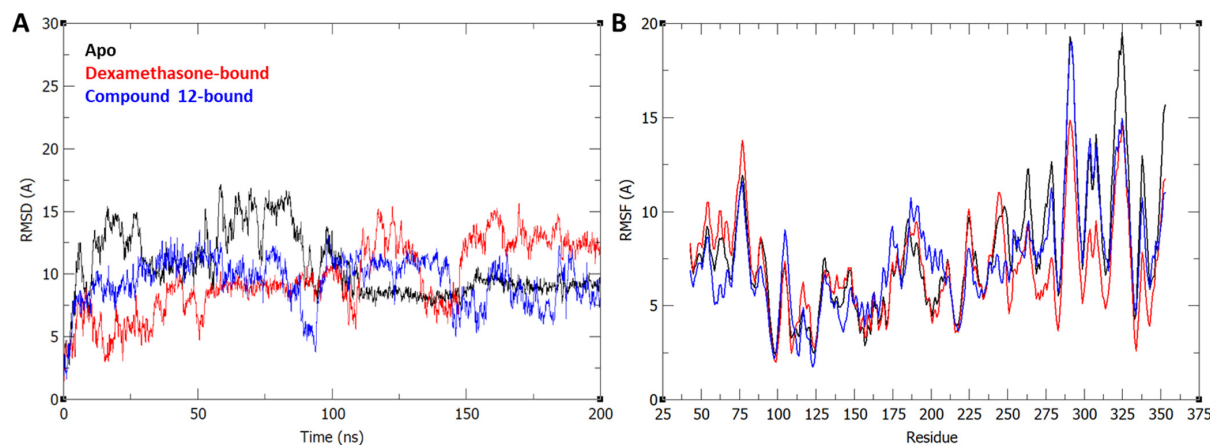


**Figure 7.** Molecular dynamics analysis of p50 apo and bound structures: (A) RMSD and (B) RMSF plot of amino acid residues of apoprotein, the p50–dexamethasone complex, and the p50–compound **12** complex.

Hydrogen bond analysis of the trajectories (Figure 8) further revealed that dexamethasone was able to maintain relatively stable hydrogen bonding interactions with p50 throughout the simulation, while 12 only had H-bonding for less than 50% of the simulation time. This suggests that 12 depends on interactions other than H-bonding to maintain binding with p50. This is consistent with the initial assessment that compound 12 displayed more vdw and alkyl interactions instead of hydrogen bonding.

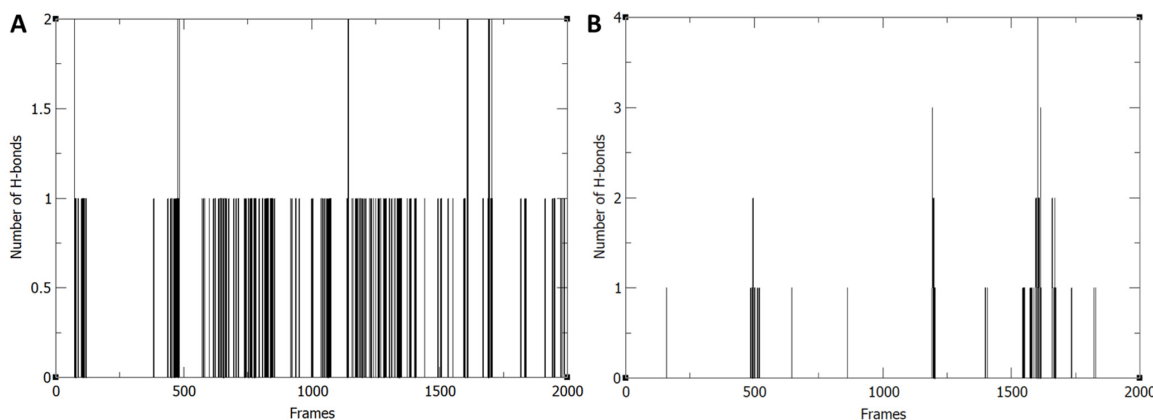


**Figure 8.** Hydrogen bonding analysis: (A) dexamethasone-bound p50 and (B) compound-**12**-bound p50.

### 3.4. Protein Energy Networks

Beyond structural flexibility alterations, it is crucial to consider the effects of ligand binding on intramolecular signaling, which may not necessarily manifest as conformational changes. Within the protein structure, certain key elements play pivotal roles in maintaining structural stability, protein activity, and signal transduction, particularly regarding allosteric binding. Betweenness centrality (BC) serves as a metric to gauge the significance of residues in transmitting information within a protein network, with higher BC values indicating greater influence over the network.

In the apo structure of p50 (Figure 9), residues exerting significant influence on intramolecular signal transmission include D209, K244, R335, and E341, while residues F56, H110, R157, E160, and R164 exhibit moderate influence over the protein energy network. Interestingly, both dexamethasone and compound **12** binding induce similar changes in the centrality landscape, notably decreasing the betweenness centrality of K244, a residue located in the linking region between the two lobes of p50. This suggests that both compounds have the potential to inhibit p50 activity by significantly constraining the central linking region and impeding residue–residue communication between the lobes of p50. This hold on the linking region may also be related to the observed instability in the protein structural conformation upon ligand binding as displayed by the RMSD and RMSF results. Additionally, dexamethasone suppresses the influence of H110, which is not observed with compound **12** binding. Nonetheless, these observations imply that these two compounds may operate through similar mechanisms when binding to p50.

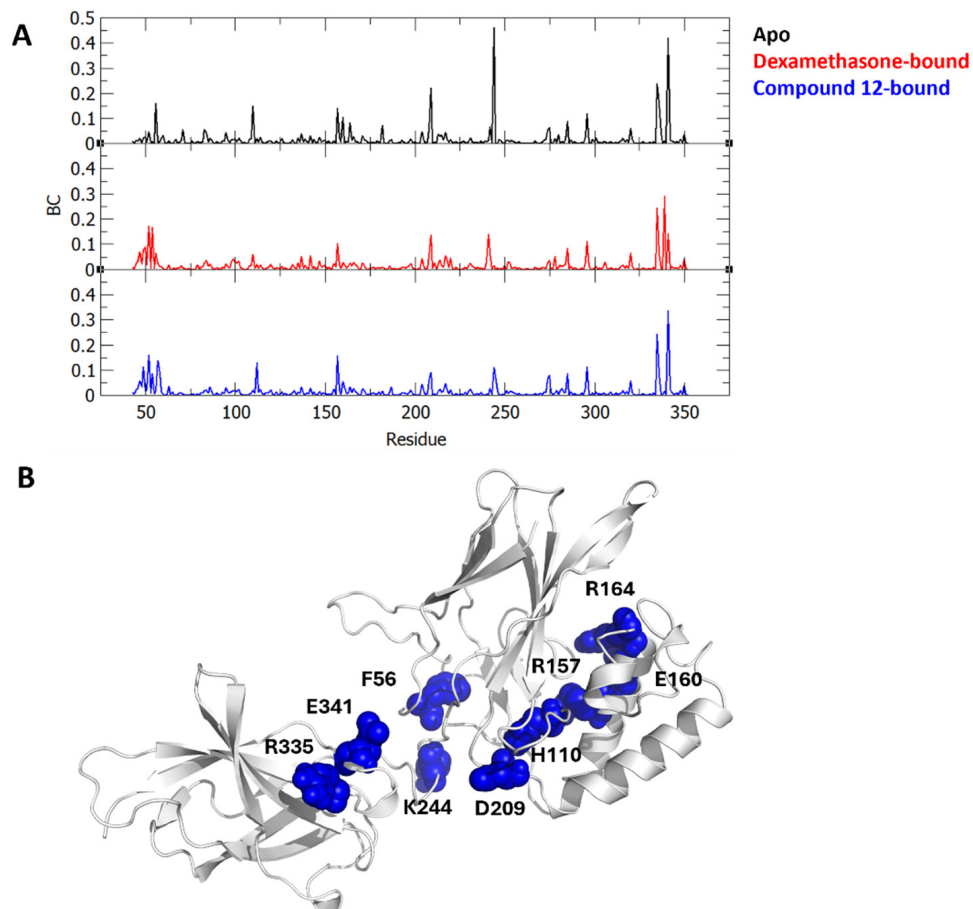


**Figure 9.** Centrality analysis for p50 structure. (A) Betweenness centrality plot of apoprotein, the p50–dexamethasone complex, and the p50–compound **12** complex. (B) p50 with moderate- to high-centrality residues shown as blue spheres.

### 3.5. Pharmacokinetic Properties of the Selected Compounds

The anticipated pharmacokinetic properties [70] of the compounds, along with the dexamethasone control, are synthesized and visualized in Figure 10 as a heatmap. Notably, all six (6) compounds demonstrate a moderate potential for metabolism by cytochrome P-450, an enzyme pivotal in metabolizing foreign substances or xenobiotics within the body. Additionally, these compounds are forecasted to exhibit moderate inhibition of P-glycoprotein, which may enhance the bioavailability of these compounds [71,72]. Furthermore, these compounds were found to be potential hERG inhibitors, which may have a tendency to exhibit moderate to low levels of genotoxicity, acute oral toxicity, QT interval prolongation, and hepatotoxicity as the side effect of being a drug [73,74]. Most of the compounds exhibited favorable physicochemical properties compared to the control, except for compound 58, which displayed limited water solubility. Consequently, compound 58 may necessitate further structural optimization, such as particle size adjustment or pH modification, potentially through nanosuspension technology or salt formation [74].



**Figure 10.** ADMET pharmacokinetic properties of the six compounds.

#### 4. Discussion

Early investigations have underscored the pivotal role of the p50 subunit in orchestrating inflammatory responses and in the pathogenesis of diseases linked to chronic inflammation, including cancer. Compounds identified as potential p50 inhibitors, with the potential to modulate immune responses, hold promise as phytochemical leads for managing various conditions associated with chronic inflammation [14,58]. In this study, six phytoconstituents (compounds **11**, **12**, **14**, **16**, **56**, and **58**) were identified as promising p50 inhibitors based on their interaction with key amino acids within the DNA-binding site. Guided by pharmacophore descriptors, these ligand molecules displayed diverse types of non-covalent interactions and varying binding affinities with the target protein [54]. Among these compounds, compound **12** exhibited the most promising protein–ligand interaction ( $-4.2$  kcal/mol), showing a less significant change in the RMSF profile of the p50 subunit complex. Interestingly, only a few amino acid residues (Arg57, Glu63, Lys244, Ala245) involved in ligand binding demonstrated significant changes in the RMSF plot (Supplementary Figure S11), suggesting the possibility of an allosteric shift in protein dynamics [70]. The binding of a ligand could also affect the thermodynamic properties of the subunit and change the local enthalpy–entropy compensation that can allow transmission of the vibration motion (or fluctuation) away from the binding site [75]. Additionally, the stability in the flexibility of compound **12**, as indicated by RMSD, suggests robust binding within the p50 DNA binding site [64]. In contrast, compound **14** displayed greater fluctuation in RMSD (greater than  $2.3$  Å), likely due to carbon–hydrogen bonding interactions ( $3.50$  Å) present in the interaction between compound **14** and the p50 subunit., highlighting the impact of hydrogen bonding patterns (e.g., carbon–hydrogen bonds) on ligand affinity and protein stability [65].

This study furnishes preliminary *in silico* data regarding the potential anti-inflammatory activity of novel compounds isolated from Philippine plants by Ragasa and co-workers between 1993 and 2020. Further enhancement of the pharmacokinetic properties of these compounds can be achieved by delineating the structure–activity relationship between their chemical structure (pharmacophore predictors) and target biological activity, prior to conducting *in vitro* and *in vivo* experiments. Once this has been determined, the part of the molecule (descriptor) that causes poor pharmacokinetics property of the compound(s) could be modified or derivatized [67,76]. The derivatives of the compound (or analogues) may have a higher specificity and lower toxicity, since binding to an alternative target has been demonstrated to be the root cause of drug toxicity. By this means, the probability of reaching and surpassing the clinical trials can be improved [77]. Additionally, exploring drug delivery systems may offer avenues to augment the bioavailability and pharmacokinetics of these druggable compounds [77,78].

#### 5. Conclusions

Research has consistently demonstrated the pivotal role of inflammation control in improving the prognosis of degenerative diseases such as cancer and those arising secondary to pathogen infections. Given the potential therapeutic benefits, plant-derived compounds have garnered significant interest within the pharmaceutical industry as a source of anti-inflammatory agents. This study investigated several candidates for their anti-inflammatory properties by assessing their binding affinity to the p50 protein. Notably, all compounds under scrutiny belong to the terpene group, known for their anti-inflammatory effects by modulating various signaling pathways involved in inflammatory responses. The study also evaluated the drug-likeness and pharmacokinetic properties of these compounds. Following initial screening and docking analyses, six compounds displayed higher or comparable binding affinity to the p50 protein compared to the dexamethasone control. Among them, compound **12** exhibited the highest binding affinity (lowest binding energy) and emerged as the most promising candidate among the shortlisted compounds. The predicted pharmacokinetic properties offer valuable insights for further investigations, such as structure–activity relationship analyses. Nonetheless, these initial *in silico* screening

findings underscore the need for subsequent in vitro and in vivo assays to validate their biological activities and pharmacokinetic profiles.

**Supplementary Materials:** The following supporting information can be downloaded at: <https://www.mdpi.com/article/10.3390/cryst14050438/s1>, Table S1: List of previously reported new or novel compounds from plants available in the Philippines, Table S2. Evolution of non-covalent bonding interaction between the protein and ligand in 10 ns, Figure S1: Binding interaction of p50 and compound 11; Figure S2: Binding interaction of p50 and compound 14; Figure S3: Binding interaction of p50 and compound 16; Figure S4: Binding interaction of p50 and compound 56; Figure S5: Binding interaction of p50 and compound 58; Figure S6: Molecular simulation of p50–compound 11; Figure S7: Molecular simulation of p50–compound 14; Figure S8: Molecular simulation of p50–compound 16; Figure S9: Molecular simulation of p50–compound 56; Figure S10: Molecular simulation of p50–compound 58; Figure S11: Amino acid residues with significant vibration motion during the simulation. See references for supplementary materials [15–44].

**Author Contributions:** Conceptualization and methodology, G.G.O.; formal analysis, writing—original draft preparation, J.U.T.; formal analysis, writing, S.J.Y.M.; review and editing, G.G.O., M.C.S.T., V.A.S.N., and V.C.L. All authors have read and agreed to the published version of the manuscript.

**Funding:** This research received no external funding.

**Data Availability Statement:** The original contributions presented in the study are included in the article/Supplementary Material, further inquiries can be directed to the corresponding authors.

**Acknowledgments:** The authors acknowledge and dedicate this work to the Late Consolacion Y. Ragasa.

**Conflicts of Interest:** The authors declare no conflicts of interest.

## References

1. Lange, B. The Evolution of Plant Secretory Structures and Emergence of Terpenoid Chemical Diversity. *Annu. Rev. Plant Biol.* **2015**, *66*, 139–159. [[CrossRef](#)] [[PubMed](#)]
2. Dillard, C.J.; German, J.B. Phytochemicals: Nutraceuticals and human health. *J. Sci. Food Agric.* **2000**, *80*, 1744–1756. [[CrossRef](#)]
3. Saleh, H.A.; Yousef, M.H.; Abdelnaser, A. The anti-inflammatory properties of phytochemicals and their effects on epigenetic mechanisms involved in TLR4/NF- $\kappa$ B-mediated inflammation. *Front. Immunol.* **2021**, *12*, 606069. [[CrossRef](#)] [[PubMed](#)]
4. Salminen, A.; Lehtonen, M.; Suuronen, T.; Kaarniranta, K.; Huuskonen, J. Terpenoids: Natural inhibitors of NF- $\kappa$ B signaling with anti-inflammatory and anticancer potential. *Cell. Mol. Life Sci.* **2008**, *65*, 2979–2999. [[CrossRef](#)] [[PubMed](#)]
5. Shin, S.A.; Joo, B.J.; Lee, J.S.; Ryu, G.; Han, M.; Kim, W.Y.; Park, H.H.; Lee, J.H.; Lee, C.S. Phytochemicals as anti-inflammatory agents in animal models of prevalent inflammatory diseases. *Molecules* **2020**, *25*, 5932. [[CrossRef](#)] [[PubMed](#)]
6. Wang, Z.P.; Cai, S.X.; Liu, D.B.; Xu, X.; Liang, H.P. Anti-inflammatory effects of a novel peptide designed to bind with NF- $\kappa$ B p50 subunit. *Acta Pharmacol. Sin.* **2006**, *27*, 1474–1478. [[CrossRef](#)] [[PubMed](#)]
7. Yu, Y.; Wan, Y.; Huang, C. The Biological Functions of NF- $\kappa$ B1 and its potential as anti-cancer target. *Curr. Cancer Drug Targets* **2009**, *9*, 566–571. [[CrossRef](#)] [[PubMed](#)]
8. Nowarski, R.; Gagliani, N.; Huber, S.; Flavell, R.A. Innate Immune Cells in Inflammation and Cancer. *Cancer Immunol. Res.* **2013**, *1*, 77–84. [[CrossRef](#)] [[PubMed](#)]
9. Vinolo, M.A.; Rodrigues, H.G.; Nachbar, R.T.; Curi, R. Regulation of inflammation by short chain fatty acids. *Nutrients* **2011**, *3*, 858–876. [[CrossRef](#)]
10. Wullaert, A. Role of NF- $\kappa$ B activation in intestinal immune homeostasis. *Int. J. Med. Microbiol.* **2010**, *300*, 49–56. [[CrossRef](#)]
11. Cartwright, T.; Perkins, N.D.; Wilson, C.L. NF $\kappa$ B1: A Suppressor of Inflammation, Ageing and Cancer. *FEBS J.* **2016**, *283*, 1812–1822. [[CrossRef](#)] [[PubMed](#)]
12. Liu, T.; Zhang, L.; Joo, D.; Sun, S.-C. NF- $\kappa$ B Signaling in Inflammation. *Signal Transduct. Target. Ther.* **2017**, *2*, 17023. [[CrossRef](#)] [[PubMed](#)]
13. Salminen, A.; Huuskonen, J.; Ojala, J.; Kauppinen, A.; Kaarniranta, K.; Suuronen, T. Activation of innate immunity system during aging: NF- $\kappa$ B signaling is the molecular culprit of inflamm-aging. *Ageing Res. Rev.* **2008**, *7*, 83–105. [[CrossRef](#)] [[PubMed](#)]
14. Chen, K.-M.; Spratt, T.E.; Stanley, B.A.; De Cotiis, D.A.; Bewley, M.C.; Flanagan, J.M.; Desai, D.; Das, A.; Fiala, E.S.; Amin, S.; et al. Inhibition of Nuclear Factor-KB DNA Binding by Organoselenocyanates through Covalent Modification of the P50 Subunit. *Cancer Res.* **2007**, *67*, 10475–10483. [[CrossRef](#)] [[PubMed](#)]
15. Ragasa, C.Y.; Padolina, W.G.; Bowden, B.F.; Li, S.; Tapiolas, D.M.; Coll, J.C. New eudesmanolide sesquiterpenes from a Philippines collection of *Wedelia prostata*. *J. Nat. Prod.* **1993**, *56*, 386–393. [[CrossRef](#)]
16. Ragasa, C.Y.; Padolina, W.G.; Yamauchi, T.; Otsuka, H.; Yamasaki, K.; Satoh, T. Germacranolides from *Pseudoelephantopus spicatus*. *Phytochemistry* **1993**, *33*, 627–629. [[CrossRef](#)]

17. Ragasa, C.Y.; Nacpil, Z.D.; Natividad, G.M.; Tada, M.; Coll, J.C.; Rideout, J.A. Tetranortriterpenoids from *Azadirachta indica*. *Phytochemistry* **1997**, *46*, 555–558. [[CrossRef](#)]
18. Ragasa, C.Y.; Rideout, J.A.; Tierra, D.S.; Coll, J.C. Sesquiterpene glycosides from *Pittosporum pentandrum*. *Phytochemistry* **1997**, *45*, 545–547. [[CrossRef](#)]
19. Ragasa, C.Y.; Rideout, J.A.; Sy, J.O.; Alcachupas, D.; Inte VM, L.; Coll, J.C. Bioactive monoterpene glycosides from *Erigeron linifolius*. *Phytochemistry* **1997**, *46*, 151–154. [[CrossRef](#)]
20. Ragasa, C.Y.; Juan, E.; Rideout, J.A. A Triterpene from *Ficus pumila*. *J. Asian Nat. Prod. Res.* **1999**, *1*, 269–275. [[CrossRef](#)]
21. Ragasa, C.Y.; Cruz, M.C.; Gula, R.; Rideout, J.A. Clerodane Diterpenes from *Tinospora rumphii*. *J. Nat. Prod.* **2000**, *63*, 509–511. [[CrossRef](#)] [[PubMed](#)]
22. Ragasa, C.Y.; Templora, V.F.; Rideout, J.A. Diastereomeric diterpenes from *Coleus blumei*. *Chem. Pharm. Bull.* **2001**, *49*, 927–929. [[CrossRef](#)] [[PubMed](#)]
23. Ragasa, C.Y.; Rideout, J.A. An antifungal cadinanolide from *Pseudoelephantopus spicatus*. *Chem. Pharm. Bull.* **2001**, *49*, 1359–1361. [[CrossRef](#)] [[PubMed](#)]
24. Ragasa, C.Y.; Tremor, N.; Rideout, J.A. Ionone derivatives from *Alternanthera sessilis*. *J. Asian Nat. Prod. Res.* **2002**, *4*, 109–115. [[CrossRef](#)]
25. Ragasa, C.Y.; Hofileña, J.G.; Rideout, J.A. New Furanoid Diterpenes from *Caesalpinia pulcherrima*. *J. Nat. Prod.* **2002**, *65*, 1107–1110. [[CrossRef](#)] [[PubMed](#)]
26. Ragasa, C.Y.; Ganzon, J.; Hofilena, J.; Tamboong, B.; Rideout, J.A. A New Furanoid Diterpene from *Caesalpinia pulcherrima*. *Chem. Pharm. Bull.* **2003**, *51*, 1208–1210. [[CrossRef](#)]
27. Ragasa, C.Y.; Tiu, F.; Rideout, J. A New cycloartenol esters from *Ixora coccinea*. *Nat. Prod. Res.* **2004**, *18*, 319–323. [[CrossRef](#)]
28. Ragasa, C.Y.; Ngo, H.T.; Rideout, J.A. Terpenoids and Sterols from *Lagerstroemia speciosa*. *J. Asian Nat. Prod. Res.* **2005**, *7*, 7–12. [[CrossRef](#)]
29. Ragasa, C.Y.; de Luna, R.D.; Cruz, W.C.; Rideout, J.A. Monoterpene Lactones from the Seeds of *Nephelium appaceum*. *J. Nat. Prod.* **2005**, *68*, 1394–1396. [[CrossRef](#)]
30. Ragasa, C.Y.; Pimenta LE, N.; Rideout, J.A. Iridoids from *Gardenia jasminoides*. *Nat. Prod. Res.* **2007**, *21*, 1078–1084. [[CrossRef](#)]
31. Ragasa, C.Y.; Tepora, M.M.; Espinelli, D.H.; Mandia, E.H.; Rideout, J. A Chromomoric acid derivatives from *Tectona philippinensis*. *J. Nat. Prod.* **2008**, *71*, 701–705. [[CrossRef](#)] [[PubMed](#)]
32. Ragasa, C.Y.; de Jesus, J.P.; Apuada, M.J.; Rideout, J.A. A New Sesquiterpene from *Artemisia vulgaris*. *J. Nat. Med.* **2008**, *62*, 461–463. [[CrossRef](#)]
33. Ragasa, C.Y.; Tsai, P.W.; Galvez, C.T.; Shen, C.C. New carvotanacetone derivatives from *Sphaeranthus africanus*. *Planta Medica* **2010**, *76*, 146–151. [[CrossRef](#)]
34. Ragasa, C.Y.; Espineli, D.L.; Shen, C.-C. New Triterpenes from *Barringtonia asiatica*. *Chem. Pharm. Bull.* **2011**, *59*, 778–782. [[CrossRef](#)]
35. Ragasa, C.Y.; Espineli, D.L.; Mandia, E.H.; Raga, D.D.; Don, M.-J.; Shen, C.-C. A New Triterpene from *Atalantia retusa* Merr. Z. *Naturforschung B* **2012**, *67*, 426–432. [[CrossRef](#)]
36. Ragasa, C.Y.; Espineli, D.L.; Shen, C.-C. Cytotoxic Triterpene from *Barringtonia asiatica*. *Pharm. Chem. J.* **2014**, *48*, 529–533. [[CrossRef](#)]
37. Ragasa, C.Y.; Espineli, D.L.; Agoo, E.M.; del Fierro, R.S. Chemical Constituents of *Cinnamomum cebuense*. *Chin. J. Nat. Med.* **2013**, *11*, 264–268. [[CrossRef](#)] [[PubMed](#)]
38. Ragasa, C.Y.; Torres, O.B.; Bernardo, L.O.; Mandia, E.H.; Don, M.J.; Shen, C.C. Glabreal-type triterpenoids from *Dysoxylum mollissimum*. *Phytochem. Lett.* **2013**, *6*, 514–518. [[CrossRef](#)]
39. Ragasa, C.Y.; Torres, O.B.; Raga, D.D.; Mandia, E.H.; Don, M.; Shen, C. New triterpenes from the bark of *Canarium asperum*. *Der Pharm. Lett.* **2014**, *6*, 290–294.
40. Ragasa, C.Y.; Espineli, D.L.; Mandia, E.H.; Don, M.-J.; Shen, C.-C. A New Triterpene from *Glinus oppositifolius*. *Chin. J. Nat. Med.* **2012**, *10*, 284–286. [[CrossRef](#)]
41. Ragasa, C.Y.; Ng, V.A.; Agoo, E.M.; Shen, C.C. An isopimarane diterpene from *Cycas sancti-lasallei*. *Sch. Res. Libr.* **2015**, *7*, 168–171.
42. Ragasa, C.Y.; Ng, V.A.S.; Agoo, E.M.G.; Shen, C.C. An isoflavanoid phloalexin and a sesquiterpene from *Cycas wadei*. *Int. J. Pharmacogn. Phytochem.* **2016**, *8*, 686–689.
43. Ragasa, C.Y.; Si, M.; Tan, M.C.S.; Pelobello, D.H.; Don, M.J.; Shen, C.C. A new sesquiterpene from *Dendranthema grandiflora* flowers. *Chem. Nat. Compd.* **2020**, *56*, 436–439. [[CrossRef](#)]
44. Barre, J.T.; Bowden, B.F.; Coll, J.C.; De Jesus, J.; De La Fuente, V.E.; Janairo, G.C.; Ragasa, C.Y. A Bioactive Triterpene from *Lantana camara*. *Phytochemistry* **1997**, *45*, 321–324. [[CrossRef](#)] [[PubMed](#)]
45. Zulueta MC, A.; Tada, M.; Ragasa, C.Y. A diterpene from *Bidens pilosa*. *Phytochemistry* **1995**, *38*, 1449–1450.
46. ACD/ChemSketch, version 2020.2.26; Advanced Chemistry Development, Inc.: Toronto, ON, Canada, 2020.
47. O’Boyle, N.M.; Banck, M.; James, C.A.; Morley, C.; Vandermeersch, T.; Hutchison, G.R. Open Babel: An Open Chemical Toolbox. *J. Cheminform.* **2011**, *3*, 33. [[CrossRef](#)] [[PubMed](#)]
48. Xiong, G.; Wu, Z.; Yi, J.; Fu, L.; Yang, Z.; Hsieh, C.; Yin, M.; Zeng, X.; Wu, C.; Lu, A.; et al. ADMETlab 2.0: An Integrated Online Platform for Accurate and Comprehensive Predictions of ADMET Properties. *Nucleic Acids Res.* **2021**, *49*, W5–W14. [[CrossRef](#)] [[PubMed](#)]

49. Trott, O.; Olson, A.J. AutoDock Vina: Improving the speed and accuracy of docking with a new scoring function, efficient optimization, and multithreading. *J. Comput. Chem.* **2010**, *31*, 455–461. [[CrossRef](#)]
50. Berendsen, H.J.C.; Van Der Spoel, D.; Van Drunen, R. GROMACS: A message-passing parallel molecular dynamics implementation. *Comput. Phys. Comm.* **1995**, *91*, 43–56. [[CrossRef](#)]
51. Schüttelkopf, A.W.; van Aalten, D.M. PRODRG: A tool for high-throughput crystallography of protein-ligand complexes. *Acta Crystallogr. Sect. D Biol. Crystallogr.* **2004**, *60 Pt. 8*, 1355–1363. [[CrossRef](#)]
52. Humphrey, W.; Dalke, A.; Schulten, K. VMD—Visual Molecular Dynamics. *J. Molec. Graph.* **1996**, *14*, 33–38. [[CrossRef](#)]
53. Abraham, M.J.; Murtola, T.; Schulz, R.; Páll, S.; Smith, J.C.; Hess, B.; Lindahl, E. GROMACS: High performance molecular simulations through multi-level parallelism from laptops to supercomputers. *SoftwareX* **2015**, *1*, 19–25. [[CrossRef](#)]
54. Schniedman-Duhovny, D.; Dror, O.; Inbar, Y.; Nussinov, R.; Wolfson, H.J. PharmaGist: A webserver for ligand-based pharmacophore detection. *Nucleic Acids Res.* **2008**, *36* (Suppl. S2), W223–W228. [[CrossRef](#)] [[PubMed](#)]
55. Discovery Studio Visualizer, version 21.1.0.20298; Dassault Systèmes Biovia Corp: Aix en Provence, France, 2020.
56. Lüthy, R.; Bowie, J.U.; Eisenberg, D. Assessment of Protein Models with Three-Dimensional Profiles. *Nature* **1992**, *356*, 83–85. [[CrossRef](#)] [[PubMed](#)]
57. Dym, O.; Eisenberg, D.; Yeates, T.O. Detection of Errors in Protein Models. In *International Tables for Crystallography: Crystallography of Biological Macromolecules*, 2nd ed.; Arnold, E., Himmel, D.M., Rossmann, M.G., Eds.; John Wiley and Sons: Chichester, UK, 2011; Volume F.
58. Benet, L.Z.; Hosey, C.M.; Ursu, O.; Oprea, T.I. BDDCS, the Rule of 5 and Drugability. *Adv. Drug Deliv. Rev.* **2016**, *101*, 89–98. [[CrossRef](#)]
59. Noreen, S.; Maqbool, I.; Madni, A. Dexamethasone: Therapeutic potential, risks, and future projection during COVID-19 pandemic. *Eur. J. Pharmacol.* **2021**, *89*, 173854. [[CrossRef](#)]
60. Dvořák, Z.; Vrzal, R.; Maurel, P.; Ulrichová, J. Differential effects of selected natural compounds with anti-inflammatory activity on the glucocorticoid receptor and NF-κB in HeLa cells. *Chem.-Biol. Interact.* **2006**, *159*, 117–128. [[CrossRef](#)] [[PubMed](#)]
61. Yu, H.; Lin, L.; Zhang, Z.; Zhang, H.; Hu, H. Targeting NF-κB pathway for the therapy of diseases: Mechanism and clinical study. *Signal Transduct. Target. Ther.* **2020**, *5*, 209. [[CrossRef](#)]
62. Lou, L.; Zhou, J.; Liu, Y.; Wei, Y.I.; Zhao, J.; Deng, J.; Dong, B.; Zhu, L.; Wu, A.; Yang, Y.; et al. Chlorogenic acid induces apoptosis to inhibit inflammatory proliferation of IL-6-induced fibroblast-like synoviocytes through modulating the activation of JAK/STAT and NF-κB signaling pathways. *Exp. Ther. Med.* **2016**, *11*, 2054–2060. [[CrossRef](#)]
63. Fernandes, E.S.; Passos, G.F.; Medeiros, R.; da Cunha, F.M.; Ferreira, J.; Campos, M.M.; Pianowski, L.F.; Calixto, J.B. Anti-inflammatory effects of compounds alpha-humulene and (−)-trans-caryophyllene isolated from the essential oil of *Cordia verbenacea*. *Eur. J. Pharmacol.* **2007**, *569*, 228–236. [[CrossRef](#)]
64. Müller, C.W.; Rey, F.A.; Sodeoka, M.; Verdine, G.L.; Harrison, S.C. Structure of the NF-κB p50 Homodimer Bound to DNA. *Nature* **1995**, *373*, 311–317. [[CrossRef](#)] [[PubMed](#)]
65. Shivanika, C.; Kumar, S.D.; Ragunathan, V.; Tiwari, P.; Sumitha, A.; Devi, P.B. PBD Molecular docking, validation, dynamics simulations, and pharmacokinetic prediction of natural compounds against the SARS-CoV-2 main-protease. *J. Biomol. Struct. Dyn.* **2022**, *40*, 585–611. [[CrossRef](#)] [[PubMed](#)]
66. Teague, S.J. Implications of protein flexibility for drug discovery. *Nat. Rev. Drug Discov.* **2003**, *2*, 527–541. [[CrossRef](#)] [[PubMed](#)]
67. Grünberg, R.; Nilges, M.; Leckner, J. Flexibility and Conformational Entropy in Protein-Protein Binding. *Structure* **2006**, *14*, 1205. [[CrossRef](#)] [[PubMed](#)]
68. Kalamantianos, K. In silico drug repurposing for coronavirus (COVID-19): Screening known HCV drugs against the SARS-CoV-2 spike protein bound to angiotensins-converting enzyme 2(ACE-2) (6M0J). *Mol. Divers.* **2022**, *23*, 1087–1099. [[CrossRef](#)] [[PubMed](#)]
69. Chen, D.; Oezguen, N.; Urvil, P.; Ferguson, C.; Dann, S.; Savidge, T. Regulation of protein-ligand binding affinity by hydrogen bond pairing. *Sci. Adv.* **2016**, *2*, e1501240. [[CrossRef](#)] [[PubMed](#)]
70. Guan, L.; Yang, H.; Cai, Y.; Sun, L.; Di, P.; Li, W.; Liu, G.; Tang, Y. ADMET-score—A comprehensive scoring function for evaluation of chemical drug-likeness. *MedChemComm* **2019**, *10*, 148–157. [[CrossRef](#)] [[PubMed](#)]
71. Arma, M.V.; Ashokraj, Y.; Dey, C.S.; Panchagnula, R. P-glycoprotein inhibitors and their screening: A perspective from bioavailability enhancement. *Pharmacol. Res.* **2003**, *48*, 347–359. [[CrossRef](#)] [[PubMed](#)]
72. Guengerich, F.P. Mechanisms of Drug Toxicity and Relevance to Pharmaceutical Development. *Drug Metab. Pharmacokinet.* **2011**, *26*, 3–14. [[CrossRef](#)]
73. Sareen, S.; Mathew, G.; Joseph, L. Improvement in solubility of poor water-soluble drugs by solid dispersion. *Int. J. Pharm. Investigig.* **2012**, *2*, 12–17. [[CrossRef](#)]
74. Kumar, A.; Jernigan, R.L. Ligand Binding Introduces Significant Allosteric Shifts in the Locations of Protein Fluctuations. *Front. Mol. Biosci.* **2021**, *8*, 733148. [[CrossRef](#)] [[PubMed](#)]
75. Laskowski, R.A.; Gerick, F.; Thornton, J.M. The Structural Basis of Allosteric Regulation in Proteins. *FEBS Lett.* **2009**, *583*, 1692–1698. [[CrossRef](#)] [[PubMed](#)]
76. Neves, B.J.; Braga, R.C.; Melo-Filho, C.C.; Moreira-Filho, J.T.; Muratov, E.N.; Andrade, C.H. QSAR-Based Virtual Screening: Advances and Applications in Drug Discovery. *Front. Pharmacol.* **2018**, *9*, 1275. [[CrossRef](#)] [[PubMed](#)]

77. Tiwari, G.; Tiwari, R.; Sriwastawa, B.; Bhati, L.; Pandey, S.; Pandey, P.; Bannerjee, S.K. Drug delivery systems: An updated review. *Int. J. Pharm. Investig.* **2012**, *2*, 2–11. [[CrossRef](#)]
78. Morimoto, J.; Miyamoto, K.; Ichikawa, Y.; Uchiyama, M.; Makishima, M.; Hashimoto, Y.; Ishikawa, M. Improvement in Aqueous Solubility of Achiral Symmetric Cyclofenil by Modification to a Chiral Asymmetric Analog. *Sci. Rep.* **2021**, *11*, 12697. [[CrossRef](#)]

**Disclaimer/Publisher's Note:** The statements, opinions and data contained in all publications are solely those of the individual author(s) and contributor(s) and not of MDPI and/or the editor(s). MDPI and/or the editor(s) disclaim responsibility for any injury to people or property resulting from any ideas, methods, instructions or products referred to in the content.